THE JOURNAL OF PHYSICAL CHEMISTRY A

Article

pubs.acs.org/JPCA

Fragmentation of Allylmethylsulfide by Chemical Ionization: Dependence on Humidity and Inhibiting Role of Water

Thana Maihom,[†,⊥] Erna Schuhfried,[*,‡,⊥] Michael Probst,[‡] Jumras Limtrakul,[†,§] Tilmann D. Märk,[‡] and Franco Biasioli[∥]

[†]Department of Chemistry and NANOTEC Center for Nanoscale Materials Design for Green Nanotechnology, Kasetsart University, Bangkok 10900, Thailand

[‡]Institute of Ion Physics and Applied Physics, University of Innsbruck, Innsbruck, Austria.

[§]PTT Group Frontier Research Center, PTT Public Company Limited, 555 Vibhavadi Rangsit Road, Chatuchak, Bangkok 10900, Thailand

[∥]IASMA Research and Innovation Centre, Fondazione Edmund Mach, Food Quality and Nutrition Area, S Michele a/A (TN), Italy

Supporting Information

ABSTRACT: We report on a previously unknown reaction mechanism involving water in the fragmentation reaction following chemical ionization. This result stems from a study presented here on the humidity-dependent and energy-dependent endoergic fragmentation of allyl methyl sulfide (AMS) upon protonation in a proton transfer reaction-mass spectrometer (PTR-MS). The fragmentation pathways were studied with experimental (PTR-MS) and quantum chemical methods (polarizable continuum model (PCM), microhydration, studied at the MP2/6-311+G(3df,2p)//MP2/6-31G(d,p) level of theory). We report in detail on the energy profiles, reaction mechanisms, and proton affinities (G4MP2 calculations). In the discovered reaction mechanism, water reduces the fragmentation of protonated species in chemical ionization. It does so by direct interaction with the protonated species via covalent binding ($C_3H_5^+$) or via association ($AMS{\cdot}H^+$). This stabilizes intermediate complexes and thus overall increases the activation energy for fragmentation. Water thereby acts as a reusable inhibitor (anticatalyst) in chemical ionization. Moreover, according to the quantum chemical (QC) results, when water is present in abundance it has the opposite effect and enhances fragmentation. The underlying reason is a concentration-dependent change in the reaction principle from active inhibition of fragmentation to solvation, which then enhances fragmentation. This amphoteric behavior of water is found for the fragmentation of $C_3H_5^+$ to $C_3H_3^+$, and similarly for the fragmentation of $AMS{\cdot}H^+$ to $C_3H_5^+$. The results support humidity-dependent quantification efforts for PTR-MS and chemical ionization mass spectrometry (CIMS). Moreover, the results should allow for a better understanding of ion-chemistry in the presence of water.

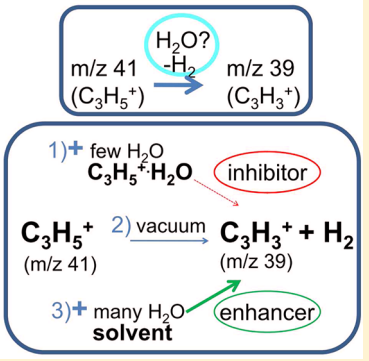

1. INTRODUCTION

Humidity influences the fragmentation pattern in chemical ionization. Moreover, in chemical ionization mass spectrometry (CIMS), humidity is involved in the complex processes taking place at and after chemical ionization. From a practical point of view, humidity in CIMS is relevant for quantification. Several general concepts are understood, such as the influence of protonated higher water clusters[1,2] and dependence on proton affinity[3,4] in CIMS. However, the underlying reaction mechanisms of how humidity influences fragmentation are often unknown and are probably reaction specific. Solvation has been proposed as one possible reaction principle, e.g., for isoprene;[5] however, it has yielded contradictory experimental results.[5] In support of our humidity dependent calibration efforts[6] and in continuation of our studies on sulfur compounds,[7,8] we set out to study humidity-dependent fragmentation.

As model compound, we choose allyl methyl sulfide (AMS). AMS belongs to the allyl sulfides, which might have preventive anticancer properties.[9] It is found in foods such as garlic,[10] onion,[11] leek, and cooked beef[12] and is also attributed to garlic breath.[10,13]

Proton transfer reaction-mass spectrometry (PTR-MS) is a mass spectrometric technique deploying soft chemical ionization with hydronium ions. It allows for direct injection analysis without sample preparation and online detection of gas phase samples.[4] Even elusive (organo)-sulfur compounds can be detected with PTR-MS,[7,14,15] down to the particularly low ppt(vol) concentration range[5] required for direct or real time (in vivo) analysis, e.g., of human breath.[13]

For the protonation reaction in the drift tube of the PTR-MS, a volatile organic compound (VOC) reacts with the hydronium ion:

Received: February 13, 2013
Revised: May 16, 2013
Published: May 17, 2013

   dx.doi.org/10.1021/jp4015806 | J. Phys. Chem. A 2013, 117, 5149−5160

$$VOC + H_3O^+ \rightarrow VOC{\cdot}H^+ + H_2O \quad (1)$$

On the basis of theoretical considerations,[16] the concentration of VOC in the sample can be calculated via the ion count rates of $VOC{\cdot}H^+$ and H_3O^+ in the mass spectrometer and the reaction rate k_{H3O+} and the (known) reaction time τ:

$$[VOC] = \frac{1}{\tau \cdot k_{H3O+}} \frac{[VOC{\cdot}H^+]}{[H_3O^+]} \quad (2)$$

Hence, in principle, PTR-MS allows for quantification without an external calibration standard. However, eq 2 is a simplification,[17,3,18] in particular because of protonated water clusters $(H_2O)_n{\cdot}H_3O^+$, which can act as reagent ions. Particular challenges in measuring compounds quantitatively with PTR-MS are fragmentation and humidity.

Measurements with PTR-MS allow for a variation of the collisional energy in the chemical reaction chamber, a flow drift tube. For instrumental intercomparison, the collisional energy is expressed as the ratio of the electric field E to the number density of the gas N in the drift tube of the PTR-MS, hence E/N, which is measured in Townsend (1 Td = 10^{-17} V·cm^2).

Fragmentation is strongly influenced by the applied collisional energy, usually thought to occur directly through the elevated energy conditions. At a higher E/N, more fragmentation occurs due to the higher energies involved.

Humidity is known to influence the protonation reactions of certain compounds in the PTR-MS,[6,19] e.g., for isoprene,[5] toluene,[19] benzene,[17,19] formaldehyde[20] (SIFDT),[21,22] alpha pinene,[23] terpenes,[1] sesquiterpenes,[24] isocyanates,[25] HCN,[26] H_2S[15,27] (SIFT), and the mix of breath gas.[28]

The choice of the collisional energy is usually a compromise between minimizing water cluster abundance, which otherwise might obscure spectra, and minimizing the amount of fragmentation at high energies.[16] Typical settings in PTR-MS for E/N are 120−145 Td. A major influence from humidity is probably the change of composition of reagent ions:

$$H_2O + H_3O^+ \leftrightarrow H_2O{\cdot}H_3O^+ \quad (3)$$

Hence, higher humidity results in the higher abundance of protonated higher water clusters $H_2O{\cdot}H_3O^+$ and $(H_2O)_n{\cdot}H_3O^+$. The protonated higher water clusters have a smaller proton affinity (PA), and hence the protonation reaction is less voluntary, or might not take place at all.[16] ΔPA of the protonation reaction (compare eq 1) is approximately equivalent to the negative change in Gibbs energy (ΔG). For efficient reactions, a minimum $\Delta PA \approx 35$ kJ/mol is required.[29]

Moreover, proton affinity has an influence on fragmentation: Reaction products from direct protonation reactions with protonated higher water clusters, as well as products from ligand switching reactions,[27] are less likely to undergo subsequent fragmentation. Again, the reason lies in the lower difference in proton affinities compared to direct hydronium ion protonation. There is less excess energy for breaking bonds in the protonated VOC; protonation is softer. Increased levels of larger protonated water clusters are found either at increased humidity in the drift tube (e.g., via humid samples) or through lower E/N. Subsequent changed fragmentation patterns due to softer reactions (via direct protonation from protonated higher water clusters or alternatively from ligand switching) have been proposed.[1,2]

In another work,[8] we investigated the collisional energy dependence of fragmentation of AMS and of other sulfides. AMS displayed a markedly different fragmentation and a rather abundant fragmentation pattern with about six major fragments (with >2% of the total ions from AMS) compared to the other small saturated organosulfur compounds, probably due to its unsaturated allyl group. We measured the collisional energy-dependent fragmentation pattern and calculated possible reaction pathways with quantum chemical (QC) methods. Comparison with literature data[5] showed differences in the found fragments and fragment abundance, which we attributed to differences in sample humidity between literature and our measurements. It indicated that humidity considerably influences fragmentation of AMS, which warranted further investigation.

Hence, in the present study, we deepen our understanding of AMS fragmentation but also use AMS as a model compound for humidity dependence. We study the influence of water vapor pressure (WVP) on the fragmentation of AMS, in combination with the effect of varying collisional energies. This corresponds to different relative humidities (RHs) and E/N ratios. We use logarithmic dilution approaches (inert gas stripping and desorption from inlet lines) to distinguish true fragments from the background. The results are compared to literature. Furthermore, we deploy extensive QC calculations for further studies on fragmentation reaction pathways. The study of the humidity dependence yields a better understanding of the influence of humidity on the fragmentation reaction, which is of importance for calibrations, both, from theory and with gas standards.

2. MATERIAL AND METHODS

2.1. Materials. The following compounds were used: allyl methyl sulfide (AMS) CAS 10152-76-8 from Aldrich (98% purity), deionized water (conductivity ≤ 0.1 μSiemens·cm^{-1}), and high purity (pa) N_2 from Rivoira (Italy).

2.2. PTR-MS Operation. A description of the PTR-MS can be found elsewhere.[4] Measurements were performed with a commercially available PTR-MS from Ionicon Analytik GmbH (Innsbruck, Austria) in the HS (high sensitivity) version equipped with a quadrupole mass analyzer as described previously (see Supporting Information S1). All signals were corrected for instrumental transmission coefficients. The fragmentation spectra were averaged typically over a minimum of 5 cycles per E/N value. Measurements from dry N_2 were performed with typically 3 cycles per E/N value. Fragment ion signals were averaged by directly calculating the percentages in relation to the protonated primary ion at each cycle and then averaging the percentages from several cycles. Isotopologue patterns, literature, and software[30,31] were used as additional aids for fragment identification. Percent fragments are usually given as % of the measured signal of m/z 89, protonated AMS, not considering isotopologues, unless stated otherwise. For details on humidity, see Supporting Information S2; for information on fragmentation in the figures, compare Supporting Information S3.

2.3. Experimental Setup. In order to achieve (pseudo)-logarithmic declining concentrations of AMS in the gas phase, inert gas stripping was used for humid samples,[7] and desorption from inlet lines was used for the dry N_2 experiment.

For the latter, after removing the AMS feed sample, desorption was induced from the inlet lines by purging with pure nitrogen (flux of 100 sccm (standard cubic centimeter per minute)). This approach resulted in a logarithmic decline of the $AMS{\cdot}H^+$ signal.[32] Attention was paid not to deplete the primary

dx.doi.org/10.1021/jp4015806 | J. Phys. Chem. A 2013, 117, 5149−5160

Table 1. Details for the Four Humidity Conditions Settings[a]

drift tube conditions	mid humid	less humid	least humid	dry (N_2)
matrix	humid N_2	humid N_2	humid N_2/air	humid N_2/air
flux N_2 [sccm]	40	200	20	100
Temperature of humidifier [°C]	30.6	25	25	
% relative humidity settings	100% @ 30.6 °C	100% @ 25 °C		0% @ 25 °C
estim. e_w [hPa][b]	44	32	21 ± 6	0
RH (of sample) @ 25 °C [%]	139	100	70 ± 20	0
estim. WVP from ion source [hPa][b]	4.2?	4.2 ± 1.7	4.2 ± 1.7	4.2 ± 1.7
ion abundance *m/z* 37 [in % *m/z* 19][c]	2.6	2.1	1.2	0.2

[a]Given for the samples, as well as corresponding calculated sample water pressure and relative humidity, an estimated value for humidity from the ion source leaking into the drift tube. An example of a reagent ion distribution is given (see Supporting Information S1 for full list) in % of H_3O^+ (*m/z* 19 monitored via its isotopologue at *m/z* 21). Least humid ion source water vapor amount is a rough estimate, hence the question mark (see Supporting Information S2 for details). e_w and φ: data with italics indicate recalculated values from ion abundance data (*m/z* 37 and 55) and italics with error range indicate estimated values. SV: switching valve of PTR-MS for SRI (switchable reagent ion); *Vp*. vapor pressure; estim., estimated; [#] recalculated from *m/z* 21 (isotopologue of H_3O^+ at *m/z* 19); *RH*, relative humidity. [b]At *T* = 25 °C and ambient pressure. [c]*E/N* ≈ 140 Td.

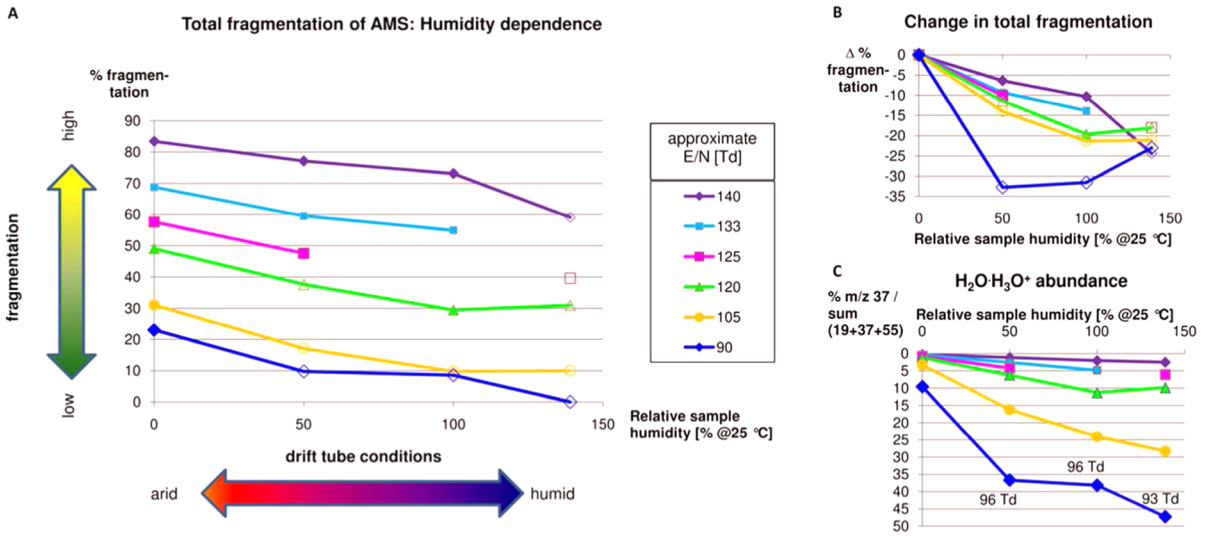

Figure 1. Total fragmentation of AMS in CIMS. Total fragmentation for the 9 most abundant signals from AMS as dependent on humidity (four settings) and for an *E/N* range of 90−140 Td. Open symbols indicate values for which some low abundant fragments could not be determined quantitatively and hence were set to zero; e.g., at low *E/N*, fragment *m/z* 55 could not be determined, and similarly, in mid humid settings for lower *E/N*, no *m/z* 61 and 55 were determined. Panel A: fragmentation is given as % of total ions from AMS from the 9 most abundant signals (*m/z* 89, 90, 91, 61, 55, 47, 41, 39, and 49 with background corrections), with *m/z* 89, 90, and 91 treated as nonfragments (isotopologues of AMS·H^+) and the others as fragments. Considering the isotopologue abundances for AMS·H^+, the maximum possible fragmentation here is 91.0%. Panel B: change in percent of total fragmentation relative to 0% RH (relative humidity). Panel C: Abundance of $H_2O{\cdot}H_3O^+$, expressed as percent of total reagent ions (*m/z* 19 + 37 + 55) for the data from panel A.

ion H_3O^+. Gas stripping and desorption effects both allow for the distinction between parent ions and derived fragments from other ions, which display a different time-dependence.[33] This is particularly important for isotopologues of $H_2O{\cdot}H_3O^+$ (*m/z* 39) and $(H_2O)_2{\cdot}H_3O^+$ (*m/z* 55).

Four settings of humidity were used (dry, least humid, less humid, and mid humid) with a humidity range of 0−140% RH @ 25 °C. Tabulated information can be found in Table 1. Further details on the PTR-MS settings and conditions for all measurements can be found in the Supporting Information S1. Because PTR-MS is also frequently used in breath gas analysis and exhaled breath is typically saturated with water vapor at ∼37 °C,[34] we prefer to call our highest humidity setting mid humid.

The water vapor content was varied as follows: During the gas stripping process, nitrogen gas takes up not only the desired VOCs but also water vapor, and thus, measurements are performed under humidified sample conditions in inert gas stripping. The water vapor content was varied by a change in the temperature of the water (25−31 °C) and the flux of the nitrogen (20−200 sccm) (standard cubic centimeter). Settings for least humid consisted of a low flux with slightly elevated amounts of parasitic reagent ions O_2^+ (*m/z* 32) and NO^+ (*m/z* 30), compared to dry N_2. However, the concentrations are still low and, in the present context, are considered not to be relevant; compare also Supporting Information S1.

2.4. Calculation of Humidity. Samples measured with saturated water vapor N_2 are considered to have 100% relative humidity at the given temperature in the humidifier (gas stripper), see Table 1.

According to Buck,[35] the temperature dependence of water vapor saturation pressure can be estimated for total pressures > 800 mbar and the relevant temperature range via

dx.doi.org/10.1021/jp4015806 | J. Phys. Chem. A 2013, 117, 5149−5160

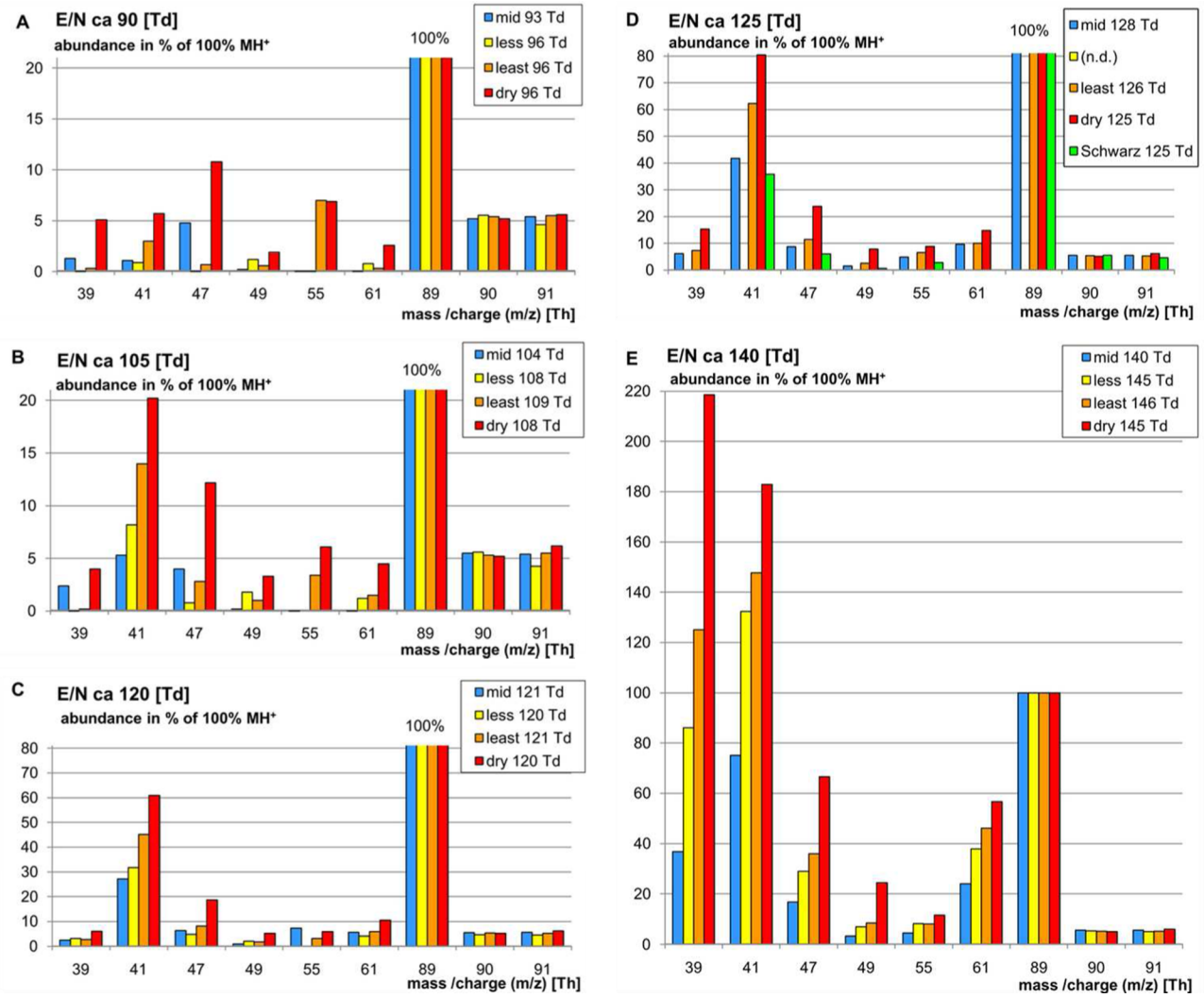

Figure 2. Humidity- and energy-dependent fragmentation patterns of AMS. Fragmentation patterns following protonation in the PTR-MS from ca. 90−140 Td (panels A−E), as % of the most abundant ions (protonated AMS at m/z 89). Four settings of humidity (dry to mid humid) were investigated. Only the main fragments are given with a cutoff at ca. 2% of total fragmentation. For comparison, the literature values (lit.) from Schwarz et al.[5] are given in panel D, which had been measured in dry nitrogen at $E/N \approx 126$ Td. n.d., not determined.

$$e_w^* = (1.0007 + 3.46\cdot10^{-6}P)\left(6.1121\cdot\exp\left(\frac{17.502\cdot T}{240.97 + T}\right)\right) \quad (4)$$

where e_w* is the saturated vapor pressure expressed in hectopascal (hPa), T is the so-called dry bulb temperature in °C, and P is the absolute pressure in hPa (assumed to be 1013.25 hPa).

The relative humidity RH (or Φ) is calculated via

$$RH = \varphi = \frac{e_w}{e_w^*}\cdot100[\%] \quad (5)$$

with e_w indicating the actual water vapor pressure in the sample and inserting e_w* from eq 4 as reference points, in particular for the temperature. By applying eqs 4 and 5, the relative humidity RH and e_w* from T = 30.6 °C were recalculated to relative humidities and e_w at 25 °C, see Table 1. Tani et al.[1] reported a linear relationship between sample water vapor pressure (WVP) and ion signal of mass 37 ($H_2O{\cdot}H_3O^+$), which we used similarly for calculating the values for least humid settings and estimating WVP from the ion source. The tabulated results for e_w and RH can be found in Table 1; for more details on the calculations, see Supporting Information S2.

2.5. Quantum Chemical Calculations. The pathways for the fragmentation of allyl methyl sulfide were calculated with the MP2 method and the 6-31G(d,p) basis set. For improved interaction energies, MP2/6-311+G(3df,2p) single-point calculations were carried out at the stationary points. Transition states were located with the Berny algorithm.[36,37] They were checked to possess one imaginary frequency corresponding to the reaction coordinate by frequency calculations at the corresponding level of theory (cf. Supporting Information S4). Because of the different approximations inherent in the functional and the effects of basis set size on thermochemistry and geometry, it is difficult to give precise error bars for the calculations. They are normally estimated to be about 5%.[38,39] The influence of humidity was investigated with both the polarizable continuum model (PCM)[40] and by explicitly including microhydration with one, two, or three water molecules along the reaction coordinate. For the calculation of proton affinities, the Gibbs free energies (ΔG) of the

dx.doi.org/10.1021/jp4015806 | J. Phys. Chem. A 2013, 117, 5149−5160

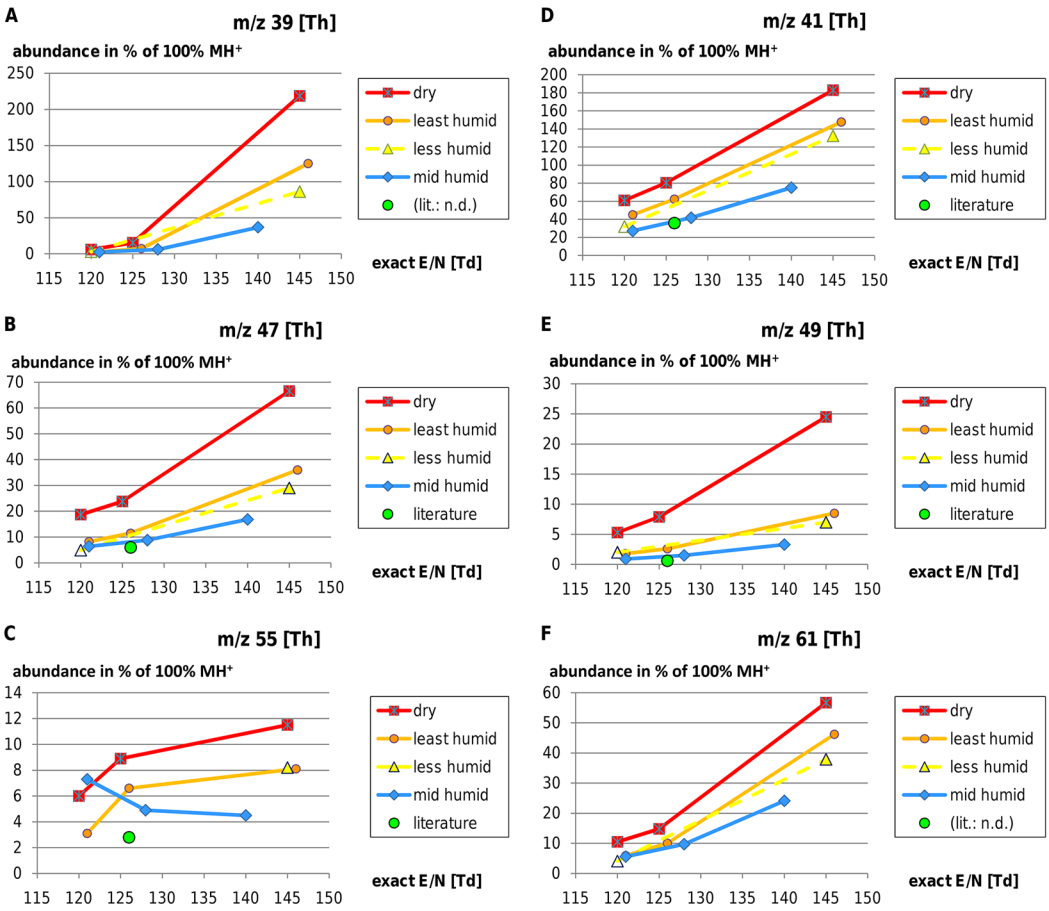

Figure 3. Energy dependence of single fragments. Collisional energy dependence of the main single ion fragments from AMS in PTR-MS plotted for four humidity ranges. Data from literature (Schwarz et al.[5]) are included for comparison; lit., literature; n.d., not determined fragment (not found). Energy range was restricted to higher *E/N*s from ca. 120−140 Td. Fragment abundance is given in % of *m/z* 89, interpreted as AMS·H^+, but not considering isotopologues. Open symbols indicate values with larger error ranges.

reactions were obtained from G4MP2 calculations.[41,42] All calculations were performed with the Gaussian09 software.[43]

3. RESULTS

3.1. Total Humidity Dependent Fragmentation of AMS in CIMS. Figure 1 demonstrates the overall humidity-dependent fragmentation of AMS in PTR-MS (panel A). Therein experimentally, humidity quantitatively reduces the overall fragmentation of AMS (AMS·H^+) in CIMS. Minor deviations can be explained as *E/N* variations and different modes of analysis of fragmentation (background correction, selection of fragments, overlap with other fragments, e.g., in the case of *m/z* 55 and 39). Compare panel B for changes in relative fragmentation. The relationship between humidity and the abundance at *m/z* 37 of the protonated first water cluster is displayed in panel C. Humidity suppresses fragmentation in the entire *E/N* range from 90 to 140 Td. *E/N* has a stronger effect on fragmentation than humidity (panel A).

3.2. Humidity and Energy Dependent Fragmentation of Single Ions from AMS in CIMS. The results for single ions for the humidity-dependent fragmentation of AMS in PTR-MS for *E/N* 90−140 Td can be seen in Figure 2. The strongest humidity-dependent fragmentation can be seen at an *E/N* ≈ 140 Td (Figure 2E). The energy dependence of single fragments can be seen in detail in Figure 3. All major fragments of AMS reactions in PTR-MS follow the same basic pattern of increased fragmentation at higher *E/N* (as expected) and decreased fragmentation at higher humidity.

3.3. Quantum Chemical Calculations for Allyl Methyl Sulfide. We study dehydrogenation reactions and minor fragmentation pathways following protonation of AMS with chemical ionization in PTR-MS (Figure 4) and investigate the humidity dependence of single fragmentation reactions (see Figures 5 and 6). The calculations complement and extend our previous calculation results.[8] Therein, we investigated with PTR-MS the fragmentation behavior of mono- and disulfides under constant humidity conditions but under varying internal energy conditions. In addition, for AMS, we deployed quantum chemical calculations in order to explain the observed major fragmentation pathways without water. Throughout this work, we assume kinetic control in the drift tube, due to the short reactions times; compare ref 8. Figure 4A gives an overview of the studied reactions, pathways *A*−*E* (using the labels from our other study[8]) and the labeling of the studied reactions R1−R5. The QC results are displayed in Figures 4B−F. The chemical reaction equations for the studied reactions are given in Table 2, including the short names used for the reactions. Additional results for the effect of humidity on the reaction R5 can be found in Supporting Information S5. In addition, the effect of humidity on the major reactions R2 (Figure 5) and R1 (Figure 6) was studied in detail with both the PCM (polarizable continuum method) (panels A in Figures 5 and 6) and with a

dx.doi.org/10.1021/jp4015806 | J. Phys. Chem. A 2013, 117, 5149−5160

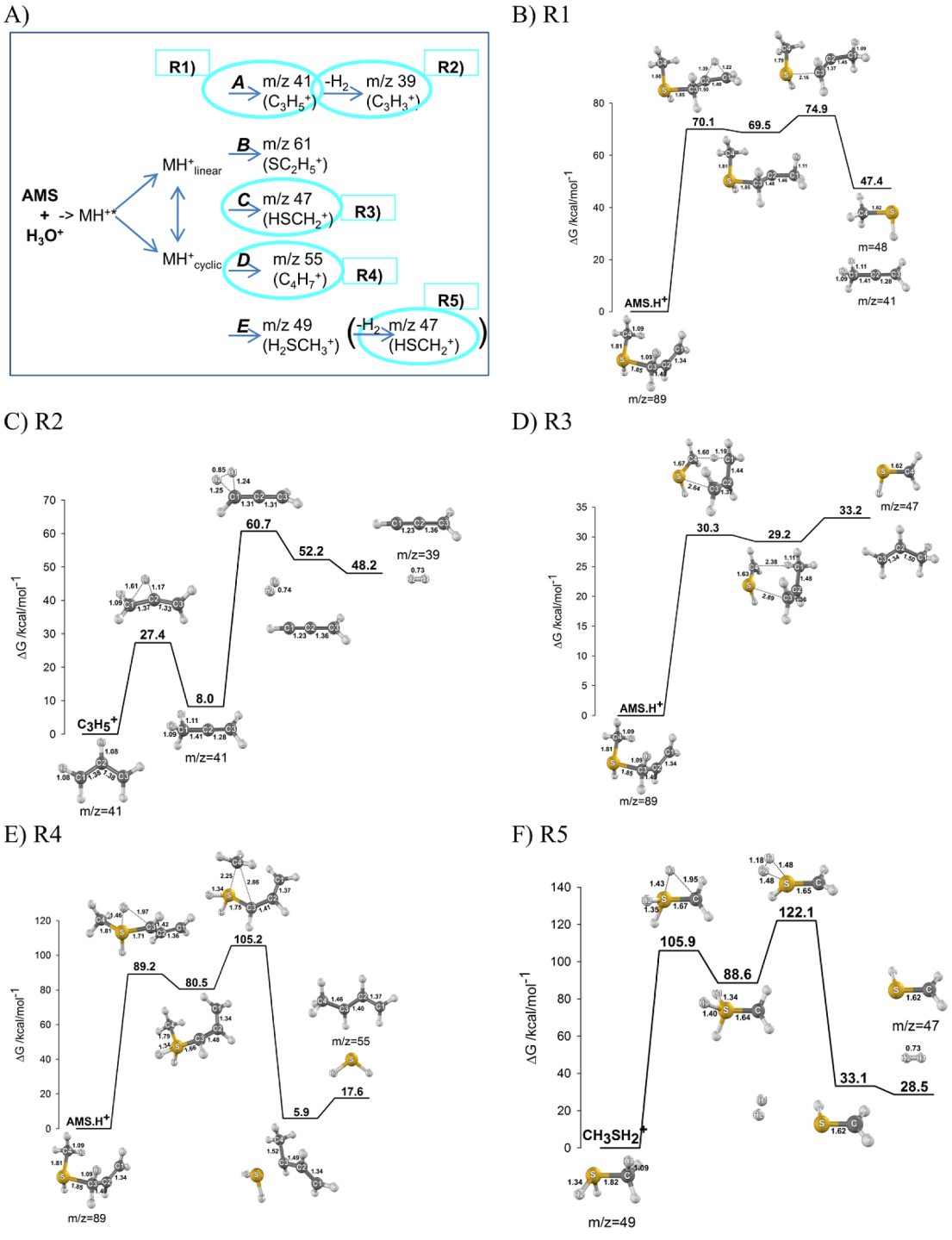

Figure 4. Energy profiles for AMS·H$^+$ fragmentation pathways. Reactions were calculated at the MP2/6-311+G(3df,2p)//MP2/6-31G(d,p) level of theory. The temperature for the Gibbs free energy ΔG is 298.15 K. Panel A: Overview of the reactions R1−R5. Panel B: conversion of AMS·H$^+$ to $C_3H_5^+$ (m/z 41) and $HSCH_3$ (m 48) (R1) in vacuum. Panel C: subsequent fragmentation (dehydrogenation) of m/z 41 to m/z 39 (R2) in vacuum. Panel D: direct fragmentation of AMS·H$^+$ to m/z 47 (R3). Panel E: fragmentation to m/z 55 (R4). Panel F: possible (but unlikely) fragmentation (dehydrogenation) of m/z 49 to m/z 47 (R5). The reaction R5 in panel D is given in parentheses because according to the quantum chemical results R3 (direct fragmentation to m/z 47) is the preferred reaction pathway.

microhydration approach where H_2O is explicitly taken into account (panels B and C in Figures 5 and 6). Further details therein can be found in Supporting Information S6, including microhydration results for three water molecules. Results on the reaction temperature dependence of calculations on hydration (both, PCM and microhydration) can be found in Supporting Information S7. Imaginary frequencies for all transition structures are given in the Supporting Information S4. Calculations for the proton affinities were performed, and the results are given in Table 3, details can be found in Supporting Information S8.

Moreover, we calculated all results in addition to the MP2 method also with the M06-2X method[44,45] (see Supporting

dx.doi.org/10.1021/jp4015806 | J. Phys. Chem. A 2013, 117, 5149−5160

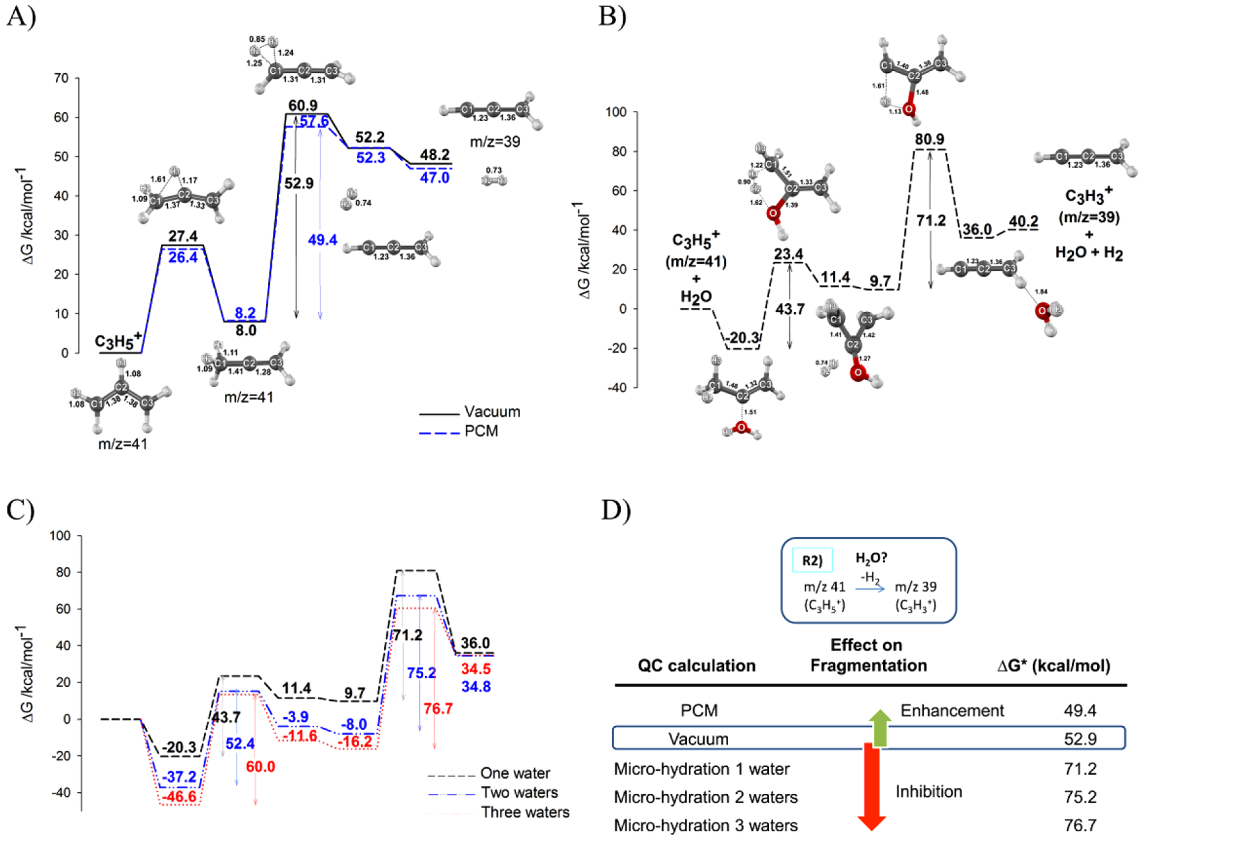

Figure 5. Humidity effect on energy profiles of the fragmentation from $C_3H_5^+$ (m/z 41) to $C_3H_3^+$ (m/z 39) (R2). Panel A: reaction energy profiles in vacuum without water (solid line) and with the PCM model (dashed line). Panel B: reaction profile for microhydration results with two water molecules. Panel C: reaction profiles comparing microhydration with one (dashed line), two (dashed-dotted line), and three (dotted line) water molecules. Panel D: comparison of the activation energies of the rate determining steps calculated for microhydration, vacuum, and PCM. Reactions were calculated at the MP2/6-311+G(3df,2p)//MP2/6-31G(d,p) level of theory. The temperature used was 298.15 K.

Information S9). The results from both methods are very close and basically the same.

4. DISCUSSION

4.1. PTR-MS Results on Combined Collisional Energy and Humidity Dependence. According to the experimental results with PTR-MS, collisional energy increases fragmentation of AMS·H^+, both in total fragmentation (Figure 1) and for the single fragments (Figure 2). Humidity reduces fragmentation, again, both overall (Figure 1) as well as for single fragments (Figures 2 and 3). The wide ranges of humidity (0−140 RH@ 25 °C) and E/N (~90−145 Td) studied cover in the most extreme cases quasi zero fragmentation at $E/N \approx 90$ Td and RH 141 [% @ 25 °C], on the one side and, on the other side, ~92% of the maximum possible fragmentation. Interestingly, humidity suppresses fragmentation by ~20−25% of the overall fragmentation (Figure 1), very uniformly (parallel graphs in Figure 1a, but see also Figure 1b) in the entire studied E/N range. We attribute this to a uniform reaction mechanism, of which the energy diagrams (activation energies) do not change (much), i.e., uniform reaction mechanisms in the fragmentation suppression of the dominating ions. Hence, presumably, with a change in water concentration, the fragmentation changes the same way for all energy (E/N) conditions.

4.2. Fragments *m/z* 47 and *m/z* 49 (R3 and R5). The fragmentation of AMS·H^+ to CH_2SH^+ (m/z 47) could in principle proceed via two different pathways,[8] either via the formation of $CH_3SH_2^+$ (m/z 49) and subsequent dehydrogenation to CH_2SH^+ (m/z 47) (R5) or via the direct formation of CH_2SH^+ (m/z 47) (R3) (compare Figure 4A). Both products, m/z 47 and 49, are found experimentally,[8] and previously,[8] we had contemplated a two-step mechanism. In this study, we go into the details of minor fragmentation pathways, such as this one, and perform quantum chemical calculations thereon.

Experimentally, the qualitative energy and humidity dependent behavior of fragment m/z 49 is similar to that of m/z 47 (Figure 3E,B), which is in contrast to the behavior of m/z 39/41 (Figure 3A,B). This different behavior might indicate that the fragment m/z 47 is rather derived directly from AMS·H^+. We therefore resorted to QC calculations on this issue.

The calculated QC reaction pathways (in vacuum) suggest a rather high activation energy for the rate determining step for the dehydrogenation reaction to m/z 47 (R5) (Figure 4F) of ΔG 105.9 kcal/mol, compared to ΔG = 30.3 kcal/mol for direct fragmentation (R3) (Figure 4D). The QC results therefore indicate that direct fragmentation from AMS·H^+ to CH_2SH^+ (m/z 47) takes place (R3), rather than dehydrogenation from $CH_3SH_2^+$ (m/z 49) (R5), and hence, the reaction R5 is set in parentheses in Figure 4A.

Interestingly, reaction R3 to m/z 47 (Figure 4D) from AMS·H^+ proceeds via a complex transition state. In the transition state, the breaking of the S−C3 bond and a proton transfer (H2) from C4 to C1 occurs, and this leads to the products CH_2SH^+ (m/z 47) and CH_2CHCH_3. This is highly reminiscent of the concerted intramolecular γ-hydrogen shift and propene elimination in the retro-ene reaction of AMS

dx.doi.org/10.1021/jp4015806 | J. Phys. Chem. A 2013, 117, 5149−5160

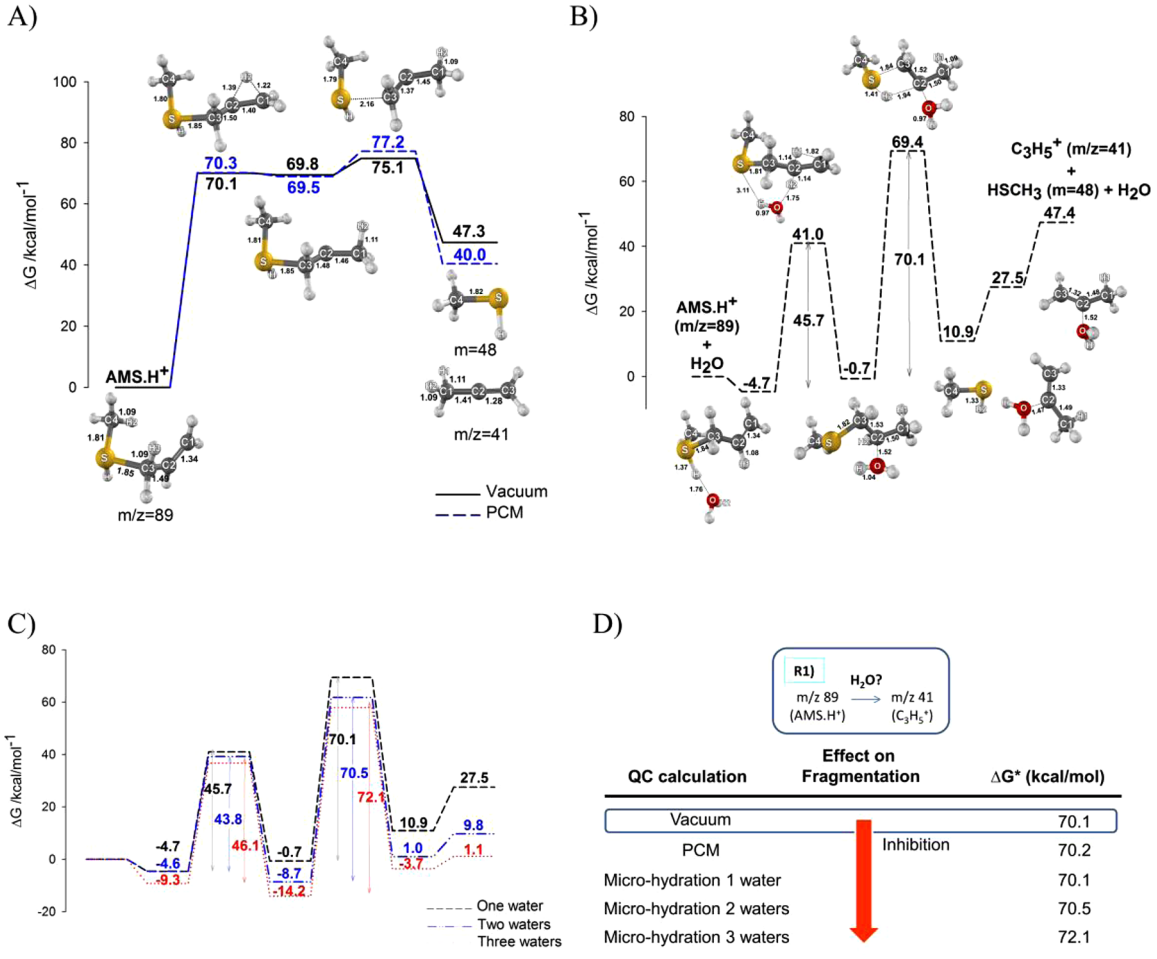

Figure 6. Humidity effect on energy profiles for the fragmentation from AMS·H$^+$ (m/z 89) to $C_3H_5^+$ (m/z 41) (R1). Panel A: reaction energy profiles in vacuum without water (solid line) and with water (dashed line) (PCM). Panel B: reaction profile for microhydration results with two water molecules. Panel C: reaction profiles comparing microhydration with one (dashed line), two (dashed-dotted line), and three (dotted line) water molecules. Panel D: activation energies of the rate determining steps from 4 QC calculations. Reactions were calculated at the MP2/6-311+G(3df,2p)//MP2/6-31G(d,p) level of theory. The temperature used was 298.15 K.

Table 2. Studied Reactions

short name	full reaction
R1	AMS·H$^+$ (m/z 89) → $C_3H_5^+$ (m/z 41) + $HSCH_3$ (m/z 48)
R2	$C_3H_5^+$ (m/z 41) → $C_3H_3^+$ (m/z 39) + H_2
R3	AMS·H$^+$ (m/z 89) → CH_2SH^+ (m/z 47) + CH_2CHCH_3
R4	AMS·H$^+$ (m/z 89) → $C_4H_7^+$ (m/z 55) + H_2S
R5	$CH_3SH_2^+$ (m/z 49) → CH_2SH^+ (m/z 47) + H_2

Table 3. Gibbs Energies (Negative Proton Affinities) of the Protonation Reactions of AMS[a]

primary ion	product	reaction	ΔG^{rxn} [kcal/mol]
H_3O^+	AMS·H$^+$	AMS + H_3O^+ ↔ AMS·H$^+$ + $2H_2O$	−38.5
H_3O^+	cAMS·H$^+$	AMS + H_3O^+ ↔ cAMS·H$^+$ + $2H_2O$	−47.6
$H_2O{\cdot}H_3O^+$	AMS·H$^+$	AMS + $H_2O{\cdot}H_3O^+$ ↔ AMS·H$^+$ + $2H_2O$	− 9.3
$H_2O{\cdot}H_3O^+$	cAMS·H$^+$	AMS + $H_2O{\cdot}H_3O^+$ ↔ cAMS·H$^+$ + $2H_2O$	−18.5

[a]The Gibbs free energies (ΔG^{rxn}) of the reactions were obtained from G4MP2 calculations at a temperature of 298.15 K. cAMS·H$^+$ is cyclic protonated AMS.

(unprotonated), calculated for pyrolysis reactions.[46] Hence, we suggest that a similar retro-ene reaction is taking place for AMS·H$^+$ fragmentation to CH_2SH^+ (m/z 47) (R3).

4.3. Fragmentation to $C_4H_7^+$ (m/z 55) (R4). $C_4H_7^+$ is a frequently encountered fragment ion from carbon chains in chemical ionization. Notably, its fragmentation reaction (R4, compare Figure 4E) has a high activation energy for the rate limiting first step (89.2 kcal/mol), yet a comparatively small endothermic total Gibbs energy of the reaction of 5.9 kcal/mol for the associated product.

4.4. Proton Affinity of AMS and the Influence of Humidity. The threshold for efficient hydronium protonation reactions in the gas phase is considered to be a difference in proton affinities of 35−40 kJ/mol[29] (corresponding to about 10 kcal/mol). AMS·H$^+$ has two isomers and the protonation reaction with H_3O^+ to both surpass the threshold (Table 3). Hence, the protonation reactions are expected to be efficient and are expected to proceed at a collisional rate, here $k \approx 2.28 \times 10^{-9}$ cm^3 s^{-1} (E/N = 140 Td; T_{drift} = 90 °C).[6] For the direct protonation reaction with the first protonated water cluster $H_2O{\cdot}H_3O^+$, the cyclic, but not the linear form, of protonated AMS provides enough energy for an efficient reaction, the linear form being borderline (compare Table 3).

dx.doi.org/10.1021/jp4015806 | J. Phys. Chem. A 2013, 117, 5149−5160

Hence, in theory, humidity-dependent changes in fragmentation patterns could be due to less available energy when proton transfer takes place from higher water clusters. However, the uniform experimental results for all *E/N* ranges for the change in overall humidity dependence (mostly caused by fragments *m/z* 41 and 39) of about 20−25% less fragmentation (compare Figure 1) with increased humidity, indicate the contrary: *E/N* has a uniform influence on humidity-dependent fragmentation of AMS·H^+. (In the literature, for ethanol a constant influence of humidity on fragmentation is seen, whereas for isoprene it is not (compare Figure 5 in ref 2).) However, the amount of protonated water clusters present decreases with increasing *E/N* (Figure 1C). This influence has been described by a roughly quadratic function; compare refs 27 and 47. Hence, a decreasing influence of protonated water clusters with increasing *E/N*, not an approximately constant influence of a reduction of ca. 20−25% in fragmentation, is expected (Figure 1A,B). Note that a small systematic change in fragmentation with *E/N* can be seen (compare Figure 1B), particularly for *E/N* ≈ 90 Td. As interpretation, we suggest that the strong uniform behavior of the humidity dependence of AMS fragmentation is not solely due to lower internal energy (caused by higher water cluster proton affinities, as reported for other compounds such as some terpenes[1]). From this, we conclude a stabilizing effect of water directly on AMS·H^+ and the fragment at *m/z* 41 $C_3H_5^+$, which consequently reduces fragmentation.

4.5. Fragment Pair *m/z* 41/39 (R2) and Its Humidity Dependence. Concerning the reaction R2, the resulting fragment at *m/z* 39 shows the strongest energy- and humidity-dependent change, and, importantly, also the largest changes (1st derivation) (Figure 3A). For calibrations, this means that this fragment is prone to introduce the largest errors in calibrations, in particular at high *E/N* and under dry conditions. A second, important fragment is *m/z* 41, by its shear abundance in the *E/N* range ∼125−145 Td. Together, these two fragments are responsible for the major part of the absolute humidity dependence of AMS fragmentation.

For modeling hydration, continuum solvent methods like the reaction field or explicit consideration of water molecules (classical or quantum chemically described) or mixtures of them can be used. First, we discuss the first and simplest approach. PCM (polarizable continuum model) is a QC method that simulates water as a polarizable continuum. All species have been reoptimized to account for solvation-induced geometrical changes. For R2, according to PCM (Figure 5A), all species become more stable with hydration. This holds true for both, the first step, the hydride shift, which is the linearization of $C_3H_5^+$ (*m/z* 41), and, to a greater extent, for the second step, the dehydrogenation. However, these QC results from PCM contradict the experimental results: According to the PCM results, the presence of water would facilitate dehydrogenation of $C_3H_5^+$ (*m/z* 41), be it as a kinetically determined reaction (which would be rather expected), but just as well for a thermodynamically controlled reaction. Thus, the experimental PTR-MS gas-phase conditions in the reaction chamber (drift tube) are not well modeled by an infinite solvent.

The counterpart to solvation in an infinite solvent is an atomistic microhydration approach, which simply means the addition of water molecules to the reacting species (compare Figure 5B). Of course, this is computationally much more challenging due to the larger size of the quantum system and the need to optimize floppy structures with multiple local minima. With single molecules of water added, a new 2-step reaction mechanism appears (see Figure 5B), in which the water molecule inhibits fragmentation: At first, water forms a covalent bond with $C_3H_5^+$ and donates a hydrogen atom for the formation of H_2. This results in the $CH_2CH_2COH^+$ intermediate. In a second reaction step, water is regenerated from the $CH_2CH_2COH^+$ intermediate, while the intermediate is converted to the $C_3H_3^+$ (*m/z* 39) product in the rate-determining step of the reaction.

A comparison of the energy profiles for adding one, two, or three water molecules as microhydration can be seen in Figure 5C. The detailed steps for one, two, and three water molecules can be seen in Supporting Information S6, S6_Figure 1. When one, two, or three water molecules are added, the activation energies for the $C_3H_5^+$ (*m/z* 41) dehydrogenation to $C_3H_3^+$ (*m/z* 39) (R2) increase for both reaction steps (see Figure 5C). This is due to a higher stability of the water−intermediate complexes. The Gibbs activation energies of the rate-determining step in microhydration (71.2, 75.2, and 76.7 kcal/mol for one, two, and three water molecules, respectively) are higher than the activation energy of $C_3H_5^+$ dehydrogenation in vacuum (49.4 kcal/mol) (Figure 5D; compare also Figure 5C to Figure 5A for vacuum without water). According to the microhydration results, the dehydrogenation reaction of $C_3H_5^+$ (*m/z* 41) to $C_3H_3^+$ (*m/z* 39) is actually inhibited by the water molecule, and this inhibition increases from one to three water molecules. Hence, in this unusual case, limited quantities of water actually act as an anticatalyst, an inhibitor: water is used and regenerated during a reaction cycle. The reaction without water has a lower activation barrier (compare summary in Figure 5D). Contrary to the continuum model, the microhydration results are in line with the experimental results and allow for the conclusion that water indeed acts as an inhibitor.

As the conditions in the drift tube, the reaction chamber of the chemical ionization, are probably proceeding at temperatures above thermal energies, also calculations for higher energies were performed; see Supporting Information S7, which basically yield the same results: microhydration is inhibited compared to vacuum.

4.6. Reaction to *m/z* 41 (R1) and Its Humidity Dependence. For the reaction of *m/z* 89 to 41, the situation of the humidity dependence is similar to that for *m/z* 39 (Figure 6). Experimental results show a stabilization with humidity against fragmentation (Figure 3D and Figure 2E). QC results for solvation in comparison to vacuum (PCM) (Figure 6A) show a tiny (ΔG = 0.1 and 2.4 kcal/mol for the first and the second steps, respectively) kinetic inhibition of fragmentation with solvation. In the microhydration scenario (cf. Figures 6B,C), the fragmentation is slightly more inhibited. All results concerning microhydration are shown in detail in Supporting Information S6.

The reaction of AMS·H^+ to $C_3H_5^+$ (*m/z* 41) proceeds also favorably in two steps (energy profiles in Figure 6C) and involves intramolecular rearrangements leading to bond breakage. The second, rate-determining step with one H_2O (70.1 kcal/mol) is similar to the vacuum system (70.1 kcal/mol). When more water is added (see Figure 6C,D for a comparison), the activation energy increases to 70.5 and 72.1 kcal/mol for two and three H_2O, respectively. This is mainly due to the stronger binding (association) of the water molecules in the intermediate complexes and is similar to the effect of H_2O in R2, the dehydrogenation of $C_3H_5^+$ (*m/z* 41) to

dx.doi.org/10.1021/jp4015806 | J. Phys. Chem. A 2013, 117, 5149−5160

$C_3H_3^+$ (m/z 39) (see Figure 5C). Here as well, microhydration inhibits fragmentation.

Again, calculations for higher ion temperatures were performed, yielding comparable results as those with thermal calculations; see Supporting Information S8.

4.7. Comparison with Literature: AMS Fragmentation Pattern and Interpretation of the Humidity Dependence Mechanism. Schwarz et al.[5] performed energy-dependent fragmentation pattern measurements for AMS with PTR-MS from dry N_2. For comparison with our results; see, e.g., Figure 2D. We can now discount our previous theory[8] that humidity is responsible for the differences in fragmentation patterns between Schwarz et al.[5] and our results. However, similar contradictory results on fragmentation pathways have been reported for isoprene,[5,2,48] which has a similar (same) fragment(s) as AMS at m/z 41 and 39.

Stabilization for a similar (same) fragment m/z 41 from isoprene by humidity was also proposed by Schwarz et al.;[5] however, the reaction mechanism was thought to be solvation. Our QC calculations with microhydration confirm the theory of stabilization (Figure 5). However, it is via a specific fragmentation−inhibitive reaction, not solvation. This could also explain the strong changes in sensitivity, in particular, when moving from completely dry samples to slightly humid samples, as reported in literature for other compounds.[17]

4.8. Relevance for Calibration Procedures. Changes in relative abundance (fragmentation) due to humidity changes are known and, in part, have been implemented as humidity-dependent calibration factors, e.g., here,[5] and the use of the ratio abundance of m/z 37/19 has been proposed[2] for better consideration of fragmentation. Alternatively, measurements at high E/N have been suggested.[6] However, PTR-MS literature is still scarce on the theory and implementation thereof for calibration considerations; compare ref 47. Currently, the focus concentrates rather on direct application of humidity calibrations to measured samples.

Recently,[6] comparison measurements of calculated data to data measured with PTR-tof-MS demonstrated that reaction rates can be well measured, even for humid conditions, as well as predicted. However, therein, E/N has to be kept above ∼120 Td, mainly because then the influence of higher water clusters can be neglected. Our results from AMS re-emphasize that quantification of PTR-MS data still requires knowledge of the fragmentation patterns and the compound-specific humidity dependence thereof.

5. CONCLUSIONS

We present a combined experimental and theoretical study on the humidity- and energy-dependent fragmentation of allyl methyl sulfide (AMS) in chemical ionization mass spectrometry (CIMS). At low humidity concentrations, as typically found in PTR-MS conditions, humidity reduces fragmentation of $AMS{\cdot}H^+$. At high concentrations of water, water would favor fragmentation of $AMS{\cdot}H^+$ according to QC calculations as the PCM results become valid at high humidity concentrations.

The reason for this amphoteric behavior of water is a change in the reaction mechanism. At high humidity concentrations, water acts as a solvent, the polarizability of the water environment facilitates fragmentation via solvation. In contrast, at low water concentrations, a different reaction mechanism takes place, in which water participates directly: the activation energy of the new rate determining step is higher because water stabilizes the complex. This makes fragmentation less likely and hence reduces the overall fragmentation. Consequently at low humidity, fragmentation is suppressed, and water acts as an inhibitor to fragmentation. This represents a new reaction mechanism of humidity in fragmentation, an inhibition against fragmentation via the direct influence of water. Furthermore, we conclude that the specific reactions of H_2O with $AMS{\cdot}H^+$ rather than changes in proton affinities or solvation are the reason for the observed humidity-dependent fragmentation patterns for AMS.

For CIMS and PTR-MS, the presented results reemphasize the importance of considering humidity- and energy-dependent fragmentation in calibrations for quantitative measurements and present a further step toward absolute calibration procedures from theory.

As humidity often influences the reaction profile of gas phase ion−molecule reactions, the newly found mechanism may be relevant in a number of fields, including upper atmospheric ion chemistry, prebiotic atmosphere of planets, ion chemistry of plasma, and plasma sources.

■ ASSOCIATED CONTENT

Ⓢ Supporting Information

Details on precursor ion settings, PTR-MS settings, and humidity settings for AMS experiments and precursor ion data of literature data. Details on the calculations of humidity. Details on the presentation of results. Imaginary frequencies of all transition structures. Quantum chemical calculations for humidity dependence of fragment m/z 49 dehydrogenation. Results of the quantum chemical calculations (microhydration) of the reactions of $C_3H_5^+$ (m/z 41) to $C_3H_3^+$ (m/z 39) and of $AMS.H^+$ (m/z 89) to $C_3H_5^+$ (m/z 41). Temperature dependence of the humidity effect on the fragmentation of $AMS{\cdot}H^+$: reaction of $C_3H_5^+$ (m/z 41) to $C_3H_3^+$ (m/z 39). Gibbs energies of AMS protonation reactions (proton affinities). Reaction profiles with the M06-2X method. High-resolution reaction profiles with the M06-2X method. This material is available free of charge via the Internet at http://pubs.acs.org.

■ AUTHOR INFORMATION

Corresponding Author

*(E.S.) E-mail: erna.schuhfried@uibk.ac.at.

Author Contributions

⊥These authors contributed equally to this work.

Author Contributions

Conceived and designed the experiments: E.S., T.M., M.P., J.L., T.D.M., and F.B. Performed the experiments: E.S., T.M., M.P., and J.L. Analyzed the data: E.S., T.M., M.P., and J.L. Contributed reagents/materials/analysis tools: E.S., T.M., M.P., J.L., T.D.M., and FB. Wrote the manuscript: E.S., T.M., M.P., J.L., T.D.M., and F.B.

Notes

The authors declare no competing financial interest.

■ ACKNOWLEDGMENTS

M.P. acknowledges support from the Austrian Ministry of Science (infrastructure grant to the LFU scientific computing platform) and from the RFBR-FWF projects 09-03-91001-a and I200-N19. J.L. and T.M. acknowledge support by grants from the National Science and Technology Development Agency (NSTDA Chair Professor and NANOTEC Center of Excellence), the Commission on Higher Education, Ministry of

Education ("the National Research University Project of Thailand (NRU)" and "the Joint Ph.D. Program Thai doctoral degree" to T.M.). This work was partly supported by Provincia Autonoma di Trento (to F.B.).

■ ABBREVIATIONS

CIMS, chemical ionization mass spectrometry; PTR-MS, proton transfer reaction-mass spectrometry; QC, quantum chemical; *m/z*, mass to charge ratio; *E/N*, ratio of the electric field to the number density of the gas in the drift tube of the PTR-MS; Td, Townsend, unit for measuring *E/N*, 1 Townsend (1 Td) = 10^{-17} V·cm^2; ppt(vol), parts per trillion (volume); sccm, standard cubic centimeter per minute (mass flow units); RH, relative humidity; WV, water vapor; WVP, water vapor pressure; PA, proton affinity; cps, counts per second; VOC, volatile organic compound; VOC·H$^+$, protonated VOC; ΔG, change in Gibbs energy; SIFDT, selected ion flow drift tube, precursor instrument of PTR-MS; tof, time-of-flight (type of mass filter in mass spectrometers); QC, quantum chemical; PCM, polarizable continuum method

■ REFERENCES

(1) Tani, A.; Hayward, S.; Hansel, A.; Hewitt, C. N. Effect of Water Vapour Pressure on Monoterpene Measurements Using Proton Transfer Reaction-Mass Spectrometry (PTR-MS). *Int. J. Mass Spectrom.* **2004**, *239*, 161−169.

(2) Keck, L.; Hoeschen, C.; Oeh, U. Effects of Carbon Dioxide in Breath Gas on Proton Transfer Reaction-Mass Spectrometry (PTR-MS) Measurements. *Int. J. Mass Spectrom.* **2008**, *270*, 156−165.

(3) de Gouw, J.; Goldan, P.; Warneke, C.; Kuster, W.; Roberts, J.; Marchewka, M.; Bertman, S.; Pszenny, A.; Keene, W. Validation of Proton Transfer Reaction-Mass Spectrometry (PTR-MS) Measurements of Gas-Phase Organic Compounds in the Atmosphere During the New England Air Quality Study (NEAQS) in 2002. *J. Geophys. Res. Atmos.* **2003**, *108*, ACH10.

(4) Lindinger, W.; Hansel, A.; Jordan, A. On-Line Monitoring of Volatile Organic Compounds at pptv Levels by Means of Proton-Transfer-Reaction Mass Spectrometry (PTR-MS): Medical Applications, Food Control and Environmental Research. *Int. J. Mass Spectrom.* **1998**, *173*, 191−241.

(5) Schwarz, K.; Filipiak, W.; Amann, A. Determining Concentration Patterns of Volatile Compounds in Exhaled Breath by PTR-MS. *J. Breath Res.* **2009**, *3* (027002), 15.

(6) Cappellin, L.; Karl, T.; Probst, M.; Ismailova, O.; Winkler, P. M.; Soukoulis, C.; Aprea, E.; Märk, T. D.; Gasperi, F.; Biasioli, F. On Quantitative Determination of Volatile Organic Compound Concentrations Using Proton Transfer Reaction Time-of-Flight Mass Spectrometry. *Environ. Sci. Technol.* **2012**, *46*, 2283−2290.

(7) Schuhfried, E.; Biasioli, F.; Aprea, E.; Cappellin, L.; Soukoulis, C.; Ferrigno, A.; Märk, T. D.; Gasperi, F. PTR-MS Measurements and Analysis of Models for the Calculation of Henry's Law Constants of Monosulfides and Disulfides. *Chemosphere* **2011**, *83*, 311−317.

(8) Schuhfried, E.; Probst, M.; Limtrakul, J.; Wannakao, S.; Aprea, E.; Cappellin, L.; Märk, T. D.; Gasperi, F.; Biasioli, F. Sulfides: Chemical Ionization Induced Fragmentation Studied with Proton Transfer Reaction-Mass Spectrometry Density Functional Calculations. *J. Mass Spectrom.* **2013**, *48*, 367−378.

(9) Wargovich, M. J. Diallylsulfide and Allylmethylsulfide Are Uniquely Effective Among Organosulfur Compounds in Inhibiting CYP2E1 Protein in Animal Models. *J. Nutr.* **2006**, *136*, 832−834.

(10) Minami, T.; Boku, T.; Inada, K.; Morita, M.; Okazaki, Y. Odor Components of Human Breath After the Ingestion of Grated Raw Garlic. *J. Food Sci.* **1989**, *54*, 763−763.

(11) Mazza, G. Relative Volatilities of Some Onion Flavor Components. *J. Food Technol.* **1980**, *15*, 35−41.

(12) Perflavory. http://www.perflavory.com/docs/doc1038781.html (accessed Mar 9, 2012).

(13) Taucher, J.; Hansel, A.; Jordan, A.; Lindinger, W. Analysis of Compounds in Human Breath after Ingestion of Garlic Using Proton-Transfer-Reaction Mass Spectrometry. *J. Agric. Food. Chem.* **1996**, *44*, 3778−3782.

(14) Soukoulis, C.; Aprea, E.; Biasioli, F.; Cappellin, L.; Schuhfried, E.; Märk, T. D.; Gasperi, F. Proton Transfer Reaction Time-of-Flight Mass Spectrometry Monitoring of the Evolution of Volatile Compounds During Lactic Acid Fermentation of Milk. *Rapid Commun. Mass Spectrom.* **2010**, *24*, 2127−2134.

(15) Feilberg, A.; Liu, D.; Adamsen, A. P. S.; Hansen, M. J.; Jonassen, K. E. N. Odorant Emissions from Intensive Pig Production Measured by Online Proton-Transfer-Reaction Mass Spectrometry. *Environ. Sci. Technol.* **2010**, *44*, 5894−5900.

(16) Lindinger, W.; Hansel, A.; Jordan, A. Proton-Transfer-Reaction Mass Spectrometry (PTR-MS): On-Line Monitoring of Volatile Organic Compounds at pptv Levels. *Chem. Soc. Rev.* **1998**, *27*, 347−354.

(17) Steinbacher, M.; Dommen, J.; Ammann, C.; Spirig, C.; Neftel, A.; Prevot, A. S. H. Performance Characteristics of a Proton-Transfer-Reaction Mass Spectrometer (PTR-MS) Derived from Laboratory and Field Measurements. *Int. J. Mass Spectrom.* **2004**, *239*, 117−128.

(18) Blake, R.; Monks, P.; Ellis, A. Proton-Transfer Reaction Mass Spectrometry. *Chem. Rev.* **2009**, *109*, 861−896.

(19) Warneke, C.; van der Veen, C.; Luxembourg, S.; de Gouw, J. A.; Kok, A. Measurements of Benzene and Toluene in Ambient Air Using Proton-Transfer-Reaction Mass Spectrometry: Calibration, Humidity Dependence, and Field Intercomparison. *Int. J. Mass Spectrom.* **2001**, *207*, 167−182.

(20) Hansel, A.; Singer, W.; Wisthaler, A.; Schwarzmann, M.; Lindinger, W. Energy Dependencies of the Proton Transfer Reactions $H_3O^+ + CH_2O \leftrightarrow CH_2OH^+ + H_2O$. *Int. J. Mass Spec. Ion Proc.* **1997**, *167−168*, 697−703.

(21) Vlasenko, A.; Macdonald, A. M.; Sjostedt, S. J.; Abbatt, J. P. D. Formaldehyde Measurements by Proton Transfer Reaction−Mass Spectrometry (PTR-MS): Correction for Humidity Effects. *Atmos. Meas. Tech.* **2010**, *3*, 965−988.

(22) Inomata, S.; Tanimoto, H.; Kato, S.; Suthawaree, J.; Kanaya, Y.; Pochanart, P.; Liu, Y.; Wang, Z. PTR-MS Measurements of Non-Methane Volatile Organic Compounds During an Intensive Field Campaign at the Summit of Mount Tai, China, in June 2006. *Atmos. Chem. Phys.* **2010**, *10*, 7085−7099.

(23) Yu, Y.; Ezell, M. J.; Zelenyuk, A.; Imre, D.; Alexander, L.; Ortega, J.; D'Anna, B.; Harmon, C. W.; Johnson, S. N.; Finlayson-Pitts, B. J. Photooxidation of α-Pinene at High Relative Humidity in the Presence of Increasing Concentrations of NOx. *Atmos. Environ.* **2008**, *42*, 5044−5060.

(24) Demarcke, M.; Amelynck, C.; Schoon, N.; Dhooghe, F.; Van Langenhove, H.; Dewulf, J. Laboratory Studies in Support of the Detection of Sesquiterpenes by Proton-Transfer-Reaction-Mass-Spectrometry. *Int. J. Mass Spectrom.* **2009**, *279*, 156−162.

(25) Gustavsson, M.; Meiby, E.; Gylestam, D.; Dahlin, J.; Spanne, M.; Karlsson, D.; Dalene, M.; Skarping, G.; Tveteråas, B. O.; Pedersen, Å. E. Adsorption Efficiency of Respirator Filter Cartridges for Isocyanates. *Ann. Occup. Hyg.* **2010**, *54*, 377−390.

(26) Knighton, W. B.; Fortner, E. C.; Midey, A. J.; Viggiano, A. A.; Herndon, S. C.; Wood, E. C.; Kolb, C. E. HCN Detection with a Proton Transfer Reaction Mass Spectrometer. *Int. J. Mass Spectrom.* **2009**, *283*, 112−121.

(27) de Gouw, J.; Warneke, C.; Karl, T.; Eerdekens, G.; van der Veen, C.; Fall, R. Sensitivity and Specificity of Atmospheric Trace Gas Detection by Proton-Transfer-Reaction Mass Spectrometry. *Int. J. Mass Spectrom.* **2003**, *223*, 365−382.

(28) Riess, U.; Tegtbur, U.; Fauck, C.; Fuhrmann, F.; Markewitz, D.; Salthammer, T. Experimental Setup and Analytical Methods for the Non-Invasive Determination of Volatile Organic Compounds, Formaldehyde and NOx in Exhaled Human Breath. *Anal. Chim. Acta* **2010**, *669*, 53−62.

(29) Bouchoux, G.; Salpin, J. Y.; Leblanc, D. A Relationship Between the Kinetics and Thermochemistry of Proton Transfer Reactions in the Gas Phase. *Int. J. Mass Spectrom. Ion Processes* **1996**, *153*, 37−48.
(30) Antolasic, F. *Elemental Composition Calculator*, version as of 9/2/2010; 2012.
(31) Antolasic, F. *Molecular Weight Calculator*, v 1.0 9/2/2010; 2012.
(32) Schuhfried, E.; Aprea, E.; Cappellin, L.; Soukoulis, C.; Viola, R.; Märk, T. D.; Gasperi, F.; Biasioli, F. Desorption Kinetics with PTR-MS: Isothermal Differential Desorption Kinetics from a Heterogeneous Inlet Surface at Ambient Pressure and a New Concept for Compound Identification. *Int. J. Mass Spectrom.* **2012**, *314*, 33−41.
(33) Aprea, E.; Biasioli, F.; Mark, T.; Gasperi, F. PTR-MS Study of Esters in Water and Water/ethanol Solutions: Fragmentation Patterns and Partition Coefficients. *Int. J. Mass Spectrom.* **2007**, *262*, 114−121.
(34) Warneke, C.; Kuczynski, J.; Hansel, A.; Jordan, A.; Vogel, W.; Lindinger, W. Proton Transfer Reaction Mass Spectrometry (PTR-MS): Propanol in Human Breath. *Int. J. Mass Spectrom. Ion Processes* **1996**, *154*, 61−70.
(35) Buck, A. L. New Equations for Computing Vapor Pressure and Enhancement Factor. *J. Appl. Meteorology* **1981**, *20*, 1527−1532.
(36) Schlegel, H. B. Optimization of Equilibrium Geometries and Transition Structures. *J. Comput. Chem.* **1982**, 214−218.
(37) Gonzalez, C.; Schlegel, H. B. An Improved Algorithm for Reaction Path Following. *J. Chem. Phys.* **1989**, *90*, 2154−2161.
(38) Hehre, W. J.; Radom, L.; Schleyer, P. von, R.; Pople, J. *Ab Initio Molecular Orbital Theory*; Wiley: New York, 1986.
(39) Friesner, R. A. Ab Initio Quantum Chemistry: Methodology and Applications. *Proc. Natl. Acad. Sci. U.S.A.* **2005**, *102*, 6648−6653.
(40) Tomasi, J.; Mennucci, B.; Cammi, R. Quantum Mechanical Continuum Solvation Models. *Chem. Rev.* **2005**, *105*, 2999−3094.
(41) Curtiss, L. A.; Redfern, P. C.; Raghavachari, K. Gaussian-4 Theory. *J. Chem. Phys.* **2007**, *126*, 084108.
(42) Curtiss, L. A.; Redfern, P. C.; Raghavachari, K. Gaussian-4 Theory Using Reduced Order Perturbation Theory. *J. Chem. Phys.* **2007**, *127*, 124105.
(43) Frisch, M. J.; Trucks, G. W.; Schlegel, H. B.; Scuseria, G. E.; Robb, M. A.; Cheeseman, J. R.; Scalmani, G.; Barone, V.; Mennucci, B.; Petersson, G. A.; et al. *Gaussian 09*, revision A.02; Gaussian, Inc.: Wallingford CT, 2009.
(44) Zhao, Y.; Truhlar, D. G. The M06 Suite of Density Functionals for Main Group Thermochemistry, Thermochemical Kinetics, Noncovalent Interactions, Excited States, and Transition Elements: Two New Functionals and Systematic Testing of Four M06-Class Functionals and 12 Other Functionals. *Theor. Chem. Acc.* **2008**, 215−241.
(45) Zhao, Y.; Truhlar, D. G. Applications and Validations of the Minnesota Density Functionals. *Chem. Phys. Lett.* **2011**, *502*, 1−13.
(46) Izadyar, M.; Gholami, M. R. Substituent Effects on the Gas Phase Reactivity of Alkyl Allyl Sulfides, a Theoretical Study. *THEOCHEM* **2006**, *759*, 11−15.
(47) de Gouw, J.; Warneke, C. Measurements of Volatile Organic Compounds in the Earth's Atmosphere Using Proton-Transfer-Reaction Mass Spectrometry. *Mass Spectrom. Rev.* **2007**, *26*, 223−257.
(48) Maleknia, S.; Bell, T.; Adams, M. PTR-MS Analysis of Reference and Plant-Emitted Volatile Organic Compounds. *Int. J. Mass Spectrom.* **2007**, *262*, 203−210.